Graduate School of Frontier Sciences, The University of Tokyo

Department of Natural Environmental Studies

Numerical Modeling for Global Environment Issues

Imasu Laboratory

School Year 2017　Master Thesis

Observation of near-surface CO_2 using synergy of TIR and SWIR spectra measured by GOSAT sensor

(GOSAT 短波長赤外・熱赤外センサーの統合解析による地表 CO_2 濃度の観測)

Submission: January, 25, 2018
Completion in March 2018

Advisor: Prof. Imasu Ryoichi

Master's Number: 47-166609

Cheng Qi

Contents

Chapter 1

Introduction

Driven by economic and population growth largely, anthropogenic greenhouse gases emissions have been increasing since the industrial era. The emission of greenhouse gases has reached 49 ± 4.5 $\mathrm{GtC}O_2\ eq/yr^3$ in 2010, which was 1.8 times larger than that in the year of 1970. A larger absolute increase could also be seen between 2000 and 2010 from Figure 1.1. Carbon dioxide (CO_2) is the biggest contributor in greenhouse gases. From 1970 to 2010, emissions of CO_2 from fossil fuel combustions and industrial processes contributed mostly and still keep a trend to increase after that. Based on the total mass of the atmosphere, the increasing of global-mean annual greenhouse gases can be expressed in terms of remaining in the atmosphere instead of being absorbed. The effect of increasing of greenhouse gases emissions, along with other anthropogenic drivers are very likely considered to have become the dominant causes of the observed global warming, which have contributed to several climate changes like precipitation changing or the melting of snow and ice in many regions (Pachauri et al., 2014).

If the continued emission of greenhouse gases is not restrained, further warming and long-lasting changes will make severe, pervasive and irreversible impacts on human's life, and even the whole ecosystem. Substantial and sustained reductions in greenhouse gases emissions should be done to limit climate change risks, which makes identification of sources and sinks of greenhouse gases become more and more important.

Obtaining the accurate information on a subcontinental scale of well-known strong greenhouse gases, especially carbon dioxide (CO_2) and methane (CH_4), has been the main purpose for controlling the global warming nowadays. With the advances in technology, satellite measurement has become one of the most effective approaches in monitoring the global distributions of greenhouse gases at high spatiotemporal resolution. The Atmospheric Infrared Sounder (AIRS) instrument launched in 2002 has observed middle and upper tropospheric CO_2 concentration with high accuracy (Maddy et al., 2008). The Orbiting Carbon Observatory 2 (OCO-2) was successfully launched in 2014 and started its observation in three channels with high-resolution spectra. Carbon Dioxide Observation Satellite Mission (TanSat) developed by China has begun its mission to monitor CO_2 from space since the

launching in July 2016, the instrument of which is a hyperspectral grating spectrometer (Liu Y et al., 2013).

Greenhouse Gases Observing Satellite (GOSAT), the first satellite which is dedicated to greenhouse gases monitoring, was launched on 23 January 2009. GOSAT is jointly developed by Japanese Ministry of the Environment, the National Institute for Environmental Studies (NIES), and the Japan Aerospace Exploration Agency (JAXA) (Yokota et al., 2004). GOSAT flies on a 666 km orbit, which is aimed at detecting weekly variation with a revisit interval of 3 days. GOSAT observes CO_2 and CH_4 by Thermal and near-infrared sensor (TANSO) which is comprised of two instruments: a Fourier Transform Spectrometer (FTS) and a Cloud and Aerosol Imager (CAI). The TANSO-FTS sensor observes shortwave infrared radiation (SWIR) and thermal infrared radiation (TIR) at the same time with a high resolution of 0.2 cm^{-1}. The former is sunlight reflected from the earth's surface and other mediums in the air and it covers spectral bands 1 through 3 between 0.758~0.775 μm, 1.56~1.72 μm and 1.92~2.08 μm. While TIR is heat radiation emitted from the atmosphere and the surface, the band of which is between 5.56~14.3 μm (Figures 1.2 and 1.3). The field of view of FTS is circular and the size of it at nadir is 10.5 km.

The products of GOSAT are divided into four parts. The FTS Level 1B data (L1B) are radiance spectra that are obtained by performing the Fourier transformation on the signals. Level 2 (L2) products provide column-averaged dry-air mole fractions of CO_2 and CH_4 (XCO_2 and XCH_4) from SWIR and vertical concentration profiles of CO_2 and CH_4 derived from TIR. Monthly averaged XCO_2 and XCH_4 data form the Level 3 product (L3). Using a global atmospheric transport model, global carbon fluxes (sources and sinks information) are released as Level 4A product (L4A).

CO_2 concentration retrieved from GOSAT TIR was compared with CO_2 data obtained by airliner observations and the differences between these two measurements were within 1 ppm on average in fall and winter in the upper troposphere (Saitoh et al., 2016). Results of GOSAT SWIR XCO_2 General Users (GU) product were biased by -0.32 ppm with a standard deviation of 1.83 ppm versus the data from the Total Carbon Column Observing Network (TCCON) and show seasonal behaviors over the northern hemisphere: higher in spring and lower in autumn (Figure 1.4; Griffith et al., 2011; Iwasaki et al., 2017). When GOSAT XCO_2 data retrieved from SWIR was compared with aircraft measurement, it showed a good agreement with aircraft-based XCO_2 and the former is biased by -0.68ppm (Inoue et al., 2013). Monthly CO_2 fluxes of 64 regions which consist of 42 subcontinental-scale terrestrial regions and 22 ocean basins were estimated from GOSAT XCO_2 retrievals. Figure 1.5 presents the monthly posterior fluxes. Positive and negative values, as colour-coded in the figure, indicate whether a region served as a net source (emission) or a sink (absorption) of CO_2 for a given month (Maksyutov et al., 2013).

More recently, it has been shown that the global XCO_2 data observed with the SWIR bands are more suitable than TIR observation to be used to place constraints on the estimating CO_2 sources and sinks (Chevallier et al., 2005; Keppel-Aleks et al., 2011; Takagi et al., 2014). However, because CO_2 is a long-lived gas, the total column measurements of CO_2 only show a primary sensitivity to synoptic-scale fluxes (Baker et al., 2010). Also, due to the transport from remote locations, the variations in the total column concentrations are only partly driven by local surface fluxes. So, the usage of XCO_2 data actually lacks a certain amount of information in the identification of CO_2 sources and sinks. The usage of XCO_2 also shows a possibility which will lead to an overestimate or underestimate of carbon uptake in different types of place (Stephens et al., 2007). For these reasons, it becomes more significant to observe lower tropospheric (LT) CO_2 concentrations, the variations of which are largely caused by surface fluxes. More accurate retrieval results of CO_2 concentrations in middle- and upper-troposphere from TIR observations were achieved (Maddy et al., 2008; Saitoh et al., 2009), whereas SWIR observations are sensitive to gas abundances in almost all the heights. The combination of TIR and SWIR observations shows a possibility in estimating LT CO_2 fluxes. M. J. Christi (2004) did a preliminary study and it shows a better result in retrieving CO_2 in the synergy of TIR and SWIR, but still lack accuracy in LT CO_2 concentration. This study provides a new method aiming at estimating CO_2 concentration under atmospheric boundary layer by a synergetic usage of GOSAT TIR and SWIR.

Atmospheric Boundary Layer (ABL), also named planetary boundary layer (PBL), is the closest to the ground within the troposphere, which is directly influenced by the existence of Earth's surface and responds to surface forcing over short time scales (Stull, 2012). In the noon, the boundary layer consists of a mixed layer which is stirred by heat radiation from the surface and convection effect from the warm moist air, and, various properties including CO_2 turn to be mixed nearly uniformly. So based on the characteristic of TIR and SWIR, more accurate retrieval results could be achieved in the middle-upper troposphere from TIR observation and XCO_2 could be retrieved from SWIR observation, it is possible to estimate the LT CO_2 concentration as long as the planetary boundary layer height (PBLH) is known.

The large difference of atmospheric constitutes concentrations between the free troposphere and well-mixed boundary layer is often used to estimate atmospheric boundary layer height (Hennemuth et al., 2006). Prijith and Rao (2016) showed the utility of vertical profiles of temperature and humidity that obtained by Cross-Track Infrared Sounder onboard Suomi National Polar-Orbiting Operational Environmental Satellite System Preparatory Project (SNPP-CrIS, Han et al., 2013) for the estimation of atmospheric boundary layer height by judging the variations of vertical gradients. This approach is employed with radiosonde measurements by Wang and Wang (2016) and determination of PBLH from the profiles of relative humidity (RH), potential temperature (θ), specific humidity (q) and refractivity (N) is shown in Figure 1.6.

The utility of XCO_2 data obtained by SWIR observation for identifying the source and sink strength of CO_2 is short of accuracy. Meanwhile, GOSAT is the first satellite that obtains vertical information of CO_2 concentrations in addition to XCO_2 in the same field of view, which makes the estimation of LT CO_2 concentration become possible. The objective of this study is to estimate CO_2 concentration in the planetary boundary layer, which hasn't been done before. The structure of this manuscript is as follows. In Sect. 2, I describe the method of calculating LT CO_2 concentration, with its function in Sect. 2.1 and detailed information of used data sources in Sect. 2.2; the retrieval method of the temperature profile is introduced in Sect. 2.3. Sect. 2.4 describe the way to determine the PBLH and Sect. 2.5 describe the modifier method to the output CO_2 profile of NIES TM. In Sect. 3, I describe the results in this research, with retrieved surface skin temperature and temperature profile results over Kanto area in Sect. 3.1. In Sect. 3.2, the preliminary results of PBLH is introduced. Sect. 3.2 is where I present the estimated LT CO_2 concentrations, containing the results from two different methods and different CO_2 profiles, also with their verification with ground-based observation. Finally, I conclude our findings in Sect. 4.

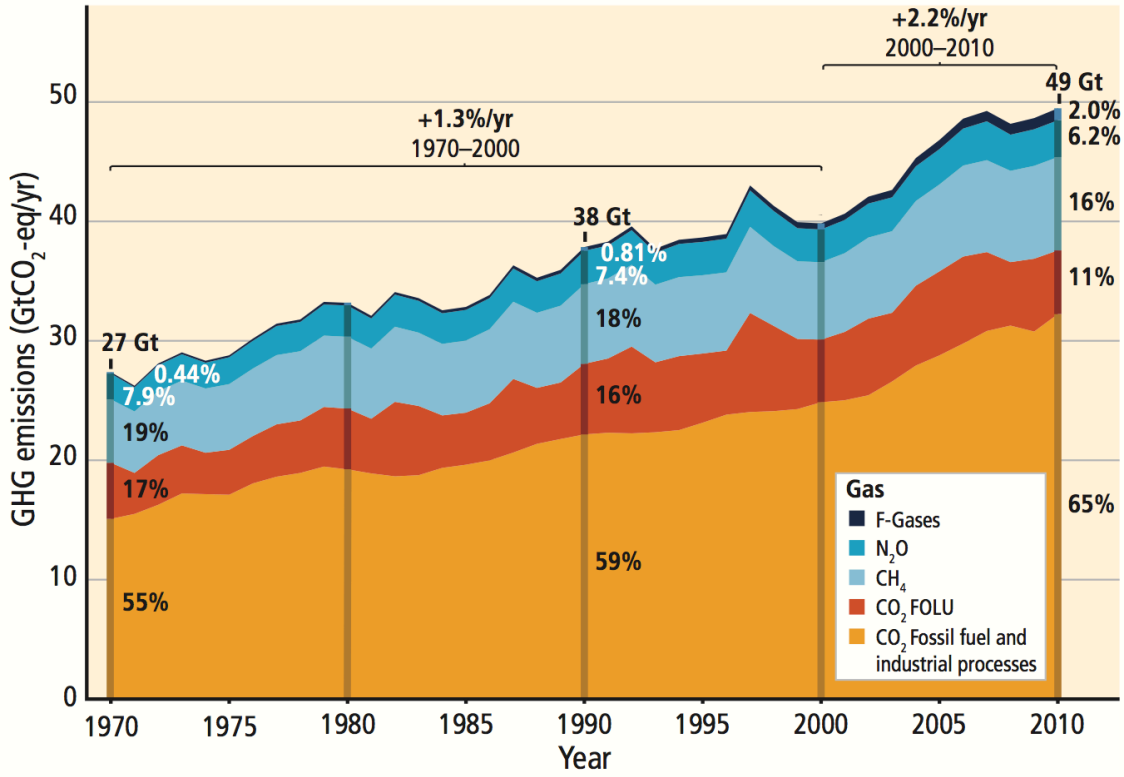

Figure 1.1. Total annual anthropogenic greenhouse gases emissions for the period 1970 to 2010 by gases. (IPCC, 2014)

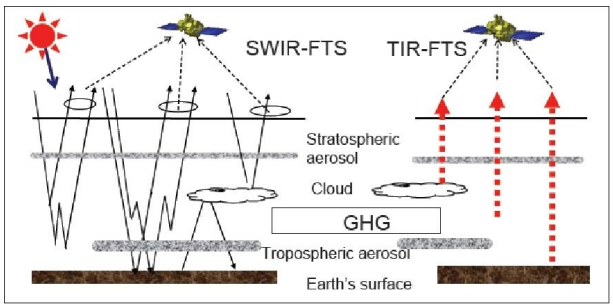

Figure 1.2. Schematic of the SWIR and TIR radiative transfer in Earth's atmosphere (image credit: JAXA, https://directory.eoportal.org/web/eoportal/satellite-missions/g/gosat)

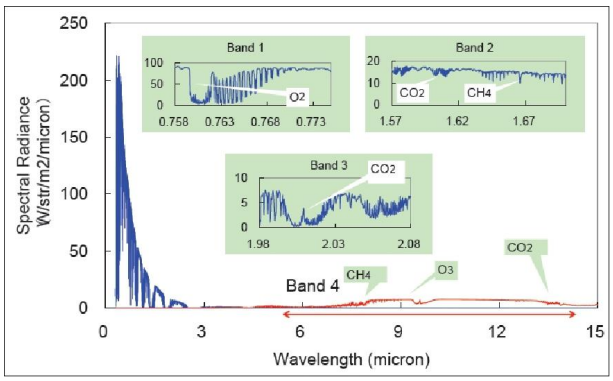

Figure 1.3. Spectral coverage of TANSO-FTS bands (image credit: JAXA, https://directory.eoportal.org/web/eoportal/satellite-missions/g/gosat)

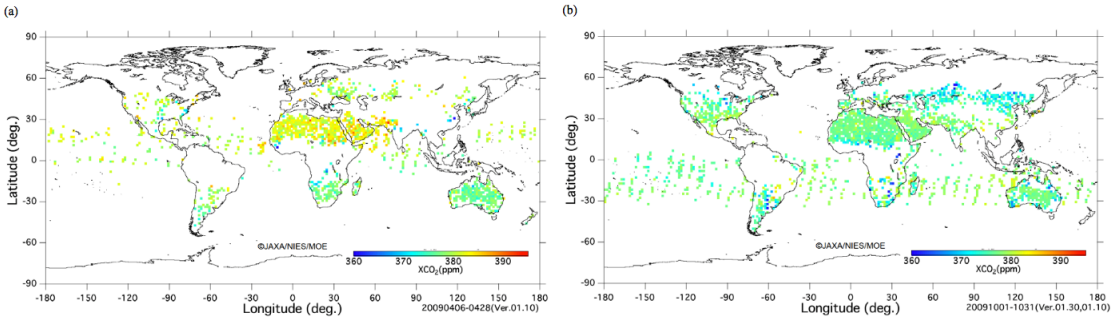

Figure 1.4. Global distribution of GOSAT SWIR XCO_2 averaged monthly in 1.5 by 1.5 degree bins for (a) April and (b) October in 2009 (Griffith et al., 2011)

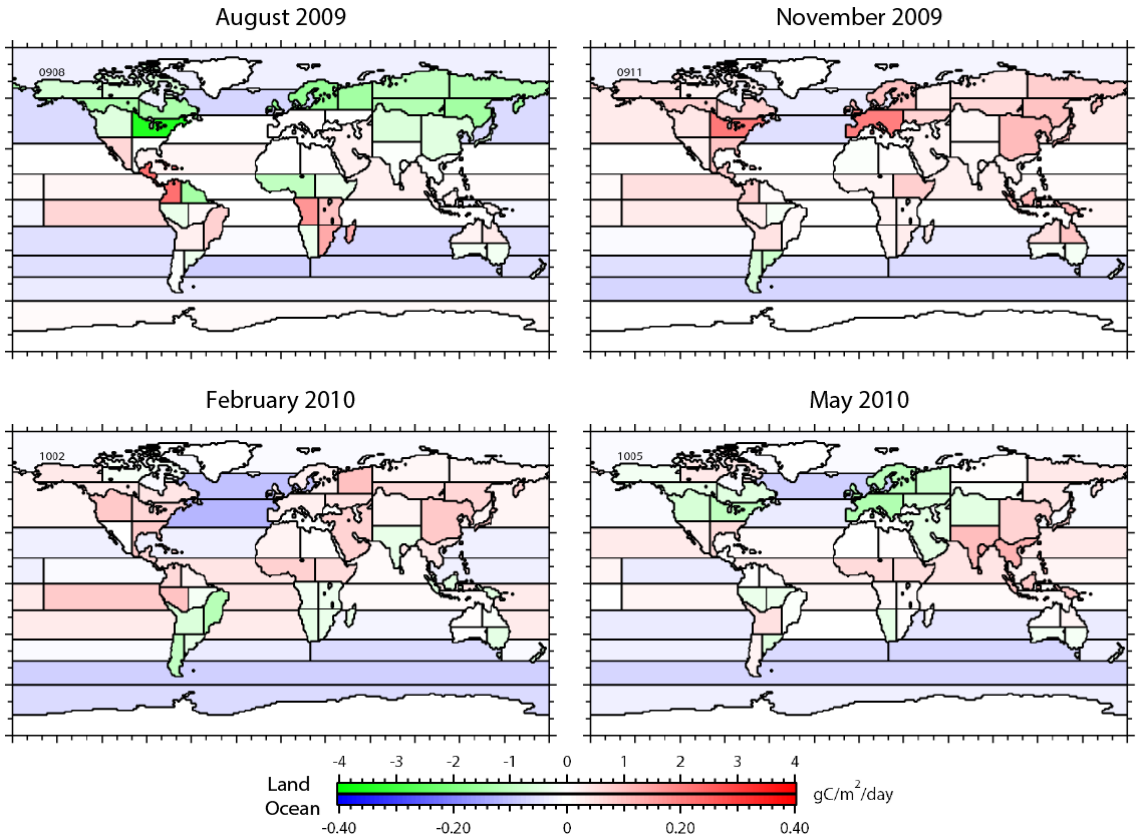

Figure 1.5. Monthly fluxes ($gCm^{-2}day^{-1}$) estimated for the 64 subcontinental regions using GV and GOSAT XCO_2 retrievals. Results for the months of August 2009 (summer in the Northern Hemisphere), November 2009 (fall), February 2010 (winter), and May 2010 (spring) are shown (Maksyutov et al., 2013)

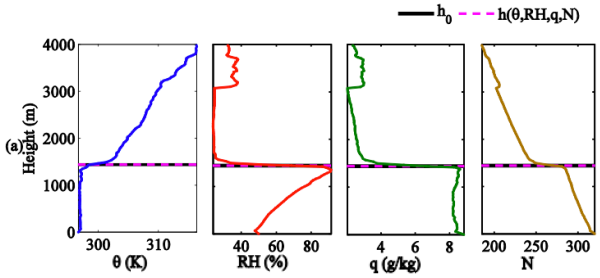

Figure 1.6. The profiles of relative humidity (RH), potential temperature (θ), specific humidity (*q*), refractivity (N) and the mixing layer height (*h*) derived from these profiles (Wang et al., 2016)

Chapter 2

Methodology

In this research, I retrieve the temperature profile from GOSAT observation, and then try to retrieve PBLH from temperature profile and finally estimate the LT CO_2 concentration in the synergetic usage of TIR and SWIR. This chapter describes the calculation method and data sets in detail used for this study. In addition, the inverse model for retrieving temperature profile is also summarized of detailed information.

2.1 Method of estimating LT CO_2

In my method, I try to estimate the LT CO_2 concentration by subtracting the upper-air CO_2 concentration above the PBL from GOSAT SWIR XCO_2. Figure 2.1 shows a schematic diagram of the principle of this method. Meanwhile, this method can only be carried out under several assumptions: (1) the atmosphere can be divided into several layers and the CO_2 concentration is uniform in each layer; (2) CO_2 concentration in the PBL is mixed uniformly. The formulation can be expressed as

$$LT\ CO_2 = \frac{XCO_2 \times P_s - \sum_{i=1}^{n}(C_i \times \Delta P_i)}{P_{PBLH} - P_s} \tag{2.1}$$

where P_s and P_{PBLH} is the atmospheric pressure at a location on Earth's surface and at planetary boundary layer height, XCO_2 is the column-averaged dry-air mole fractions of CO_2 from GOSAT SWIR L2 standard product, C_i and ΔP_i is the modified CO_2 concentration and occupied pressure at each layer height.

The ground-based observation data of CO_2 is used to verify the accuracy of the calculated LT CO_2 concentration.

2.2 Datasets

2.2.1 GOSAT data

The XCO_2 data I used is GOSAT CO_2 level 2 (L2) standard products from column abundance retrieved from Shortwave infrared radiation (SWIR) spectra (version V02.21 (2009-2014.05); V02.31 (2014.06-2014.12); V02.40 (2015.02-2015.07); V02.50 (2015.08); V02.60 (2015.09-2016.12)). The latest data processing and the auxiliary information are described in GOSAT Data Archive Service (GDAS, https://data2.gosat.nies.go.jp/index_ja.html).

I analyzed GOSAT XCO_2 data over the Kanto area in Japan. About 7 years of data from April 2009 to December 2016 (~900 scans) was used in this study.

GOSAT L1B data from Thermal infrared radiation (TIR) spectra was used to retrieve the temperature profile over Kanto area in Japan. L1B data is also from April 2009 to December 2016 (~1599 scans after cloud screening).

2.2.2 Numerical simulation

CO_2 concentration vertical profiles are the model-simulated three-dimensional concentrations from a National Institute for Environmental Studies offline tracer Transport Model (NIES TM), which has been used to simulate seasonal and diurnal cycles, synoptic variations, and spatial distributions of long-lived atmospheric constituents. The transport algorithm of the model was semi-Lagrangian, and a mass fixer was adopted to conserve the total mass of tracers for long-term simulation. The vertical mixing by boundary layer turbulence and penetrative convection are parameterized (Maksyutov et al., 2008). Since the launch of GOSAT, the output vertical profile from NIES TM has been used as a priori concentration data for operational near-real-time retrieval analyses of gas concentrations in TIR and SWIR spectra, and they are provided to users as a reference embedded in the standard products. These output profiles are possible ones to be used to estimate upper air concentration of CO_2.

High-resolution meteorological dataset from the Gird Point Value (GPV), developed by the Japan Meteorological Agency, are used for nudging in calculations by NIES TM. So, NIES TM is also set to a spatial resolution of 0.5°×0.5° in the horizontal, 21 pressure levels and a time interval of 3 hours.

2.2.3 Ground-based observations

CO_2 ground-based observation data in this study is used to verify the accuracy of estimated LT CO_2 concentration and the data are mainly provided from two sources: Meteorological tower (lat 36°04′N, lon 140°07′E, 25 m a.s.l) in Tsukuba, central Japan, by the Japan Meteorological Agency; ground based in situ measurement data by Dr. Ishidoya of National Institute of Advanced Industrial Science and Technology (AIST, lat 36°03′N, lon 140°07′E).

CO_2 Observations from the meteorological tower were from 2009 to 2013 at a height of 1.5 m and ground-based in situ measurement by AIST were provided during a period from 2014 to 2016.

2.2.4 Radiosonde

Radiosondes are instruments used for meteorological observation suspended from weather balloons. The atmospheric conditions (e.g., pressure, temperature, humidity) up to altitudes of around 30km from the ground can be observed. The radiosonde measurements data over Tsukuba area (lat 36°03.5′N, lon 140°07.5′E) is used here to evaluate the quality of the retrieved temperature profiles. The observation is conducted by the Japan Meteorological Agency and carried out daily at regular intervals worldwide (at 0900 and 2100 JST).

Comparison between retrieved temperature profile from GOSAT and radiosonde profiles is conducted with a spatial distance within 50 km and a temporal window within 5 hours from GOSAT observation.

2.3 Retrieval algorithm

2.3.1 Forward model

The Line-by-Line Radiative Transfer Model (LBLRTM, v12.4) was used in the retrieval algorithm as the forward model. LBLRTM is an accurate model which is also efficient and highly flexible. LBLRTM can be used for the calculation of spectral radiance over the whole spectral range from ultra-violet to the microwave (Clough et al., 1992, 2005). Because of the high accuracy against high-resolution spectral measurements, LBLRTM is widely used for retrieving atmospheric constituents as the foundation. High Resolution Transmission (HITRAN) database which is recognized as an international standard for a vast array of applications provides the line-by-line parameters in LBLRTM. The input parameter file in LBLRTM includes all the input parameters of spectral ranges/intervals, atmospheric layers, temperature profiles and gas profiles, the details of which are summarized in Table 2.1.

Table 2.1 Input parameters and details of forward calculations

Parameters	Retrieval	Forward Simulation
Spectral ranges	690-760 cm^{-1}	690-760 cm^{-1}
Spectral interval	0.0002 cm^{-1}	0.005 cm^{-1}
Atmospheric layers	78	111
Pressure and temperature profiles	GPV data	U.S. standard atmosphere
Gas profiles (H_2O, CO_2, O_3, N_2O, CO, etc.)	Numerical simulation (NIES TM)	U.S. standard atmosphere

2.3.2 Retrieval model

The detailed physics is often approximated by some forward model $\boldsymbol{F}(\boldsymbol{x})$. So, the relationship between measurement $\boldsymbol{y}$ (e.g. radiance spectral from GOSAT) and the state $\boldsymbol{x}$ (e.g. temperature profiles) which needs to be retrieved could be written as

$$y = F(x, b) + \epsilon = Kx + \epsilon \tag{2.2}$$

where the $\boldsymbol{y}$ is the measurement with error $\boldsymbol{\epsilon}$, and $\boldsymbol{F}(\boldsymbol{x})$ is a valued function of the unknown state $\boldsymbol{x}$ and of some other parameters $\boldsymbol{b}$ which are not included in the retrieval process, but those quantities influence the measurement. $\boldsymbol{K}$ could be defined as a $m \times n$ matrix (Jacobian matrix), not necessary square but each element in it is partial derivative of the forward model. The error term $\boldsymbol{\epsilon}$ is generally a purely random term, in other words, the sum of contributions from all sources like systematic errors. Bayesian approach is used to solve this inverse problem (Rodgers, 2000). All the real measurements have experimental noise, so a given measurement $\boldsymbol{y}$ is assumed as the Gaussian distribution with error covariance $\boldsymbol{S_\epsilon}$. The forward model provides a priori profile $\boldsymbol{x_a}$ for the state $\boldsymbol{x}$ and also its error covariance $\boldsymbol{S_a}$. The form of the description of probability density functions (*pdf's*) of state $\boldsymbol{x}$ could be expressed as

$$P(x) = \frac{1}{(2\pi)^{n/2}|S_a|^{1/2}} exp\left\{-\frac{1}{2}(x - x_a)^T S_a^{-1}(x - x_a)\right\} \tag{2.3}$$

where $\boldsymbol{x}$ comprises *n* elements. Associate with Eq. (2.2), the *pdf* of measurement $\boldsymbol{y}$ is of the form

$$P(y|x) = \frac{1}{(2\pi)^{m/2}|S_\epsilon|^{1/2}} exp\left\{-\frac{1}{2}[y - F(x)]^T S_\epsilon^{-1}[y - F(x)]\right\} \tag{2.4}$$

where $\boldsymbol{y}$ consists of m elements. Maximum a Posteriori solution (MAP) provides the most straightforward way to attach the most likely state from measurements which is described by a probability density function. Obtaining Bayes' theorem as the relationship between these two parameters $\boldsymbol{P(x)}$ and $\boldsymbol{P(y|x)}$, it states that

$$P(x|y) = \frac{P(y|x)P(x)}{P(y)} \tag{2.5}$$

where the dominator $\boldsymbol{P(y)}$ is only a normalising factor in practice. When the posterior pdf $\boldsymbol{P(x|y)}$ is also a Gaussian distribution with expected value $\hat{\boldsymbol{x}}$, we can substitute Eqs. (2.3) and (2.4) in Eq. (2.5). The expected value $\hat{\boldsymbol{x}}$ would be written

$$\hat{x} = x_a + (K^T S_\epsilon^{-1} K + S_a^{-1})^{-1} K^T S_\epsilon^{-1} (y - K x_a) \tag{2.6}$$

As the retrieval algorithm described above, the a priori covariance matrix $\boldsymbol{S_a}$ and the measurement covariance matrix $\boldsymbol{S_\epsilon}$ are set up as follows. In the retrieval of temperature, surface skin temperature and atmospheric temperature profile are retrieved simultaneously. The a priori uncertainties of surface skin temperature and profiles are assumed to be the same with a value of 3K at each altitude, which accounts for the square roots of the diagonal elements of the covariance matrix. The off-diagonal elements are all set to 0. For the Jacobian matrix are calculated as $K = \frac{\delta T_B}{\delta T}$, where $\boldsymbol{T_B}$ is the brightness temperature. The measurement covariance matrix is assumed to be a diagonal matrix with the diagonal elements corresponding to the noise of 0.5K.

Averaging kernel matrix $\boldsymbol{A}$ is defined (Rodgers, 2000) as

$$A = (K^T S_\epsilon^{-1} K + S_a^{-1})^{-1} K^T S_\epsilon^{-1} K \tag{2.7}$$

Averaging kernel matrix indicates the extent of how the retrieved quantities are sensitive to the true atmospheric state over each height range. The summation of all the elements of a row vector $\boldsymbol{A}$ is called averaging kernel area (AK area). The sensitivity could be judged from AK areas by the value of unity.

2.4 Estimation of Planetary Boundary Layer Height

Planetary boundary layer (PBL) has two characteristics: wind is turbulent and gusty within the PBL and atmosphere temperature is more dominated by advection and thermal energy budgets within

the PBL. The top of the PBL is often marked with a temperature inversion, a change in air mass, a hydrolapse and a change in wind speed/direction. Meanwhile, the height of PBL in most diagnostic analyses was determined from temperature profiles or occasionally wind.

Potential temperature θ is the actual temperature that would attain if it is adiabatically brought to a standard reference pressure P_0 , the function of which is often given by

$$\theta = T(\frac{P_0}{P})^{R/C_p} \tag{2.8}$$

where T is the current absolute temperature profiles, the unity of which is K, R is the gas constant of air, and C_p is the specific heat capacity at a constant pressure. For meteorology, R/C_p equals to 0.286. Because of the heat delivery at the ground, the potential temperature starts from a maximum value and then keeps uniform across the PBL, which shows a high degree of mixing. It makes the height of PBL become an important parameter in the assessment of air quality and pollutants dispersion. An origin method of determination of PBLH developed by Heffter (1980) shows a possibility to indicate the top of PBL by distinguishing the existence of a critical elevated inversion of potential temperature profiles. The potential temperature profiles considered in GOSAT data are not continuous, but in 78 layers, so PBLH is determined as the altitudes of maximum the second derivative of the profiles

$$Maximum\ \left\{\frac{d^2f}{dx^2} \sim \frac{f(x+z)-2f(x)+f(x-z)}{z^2}\right\} \tag{2.9}$$

where $f(x)$ relates the altitude x to the potential temperature θ; z is the interval height around x. Also, the condition that value of the second derivative should be larger than $3.5\times10e^{-6}$ is set for excluding near-linear cases.

2.5 Modification of CO_2 profile

Because the setting of the growth rate of CO_2 in the NIES TM is only 1.3 ppmV/year, which is much lower than the realistic condition (around 1.9ppmV/year), the output CO_2 profiles value turns to be lower and lower as time goes on, especially in the stratosphere. This situation is also proved by comparing averaged column value of the output and GOSAT SWIR XCO_2 value (Figure 2.2). In order to solve this problem, two methods are used to solve this problem.

The first method is to fill the blank of CO_2 concentration in each layer according to the time difference between the launching time of GOSAT and observation time, which could be expressed as

$$C_i = C_i' + \Delta C = C_i' + a \times \Delta t + b \tag{2.10}$$

where Δt is the time difference. a is the coefficient of the time difference and b is a constant value which represents the concentration difference at the first time. a and b are set to 0.5 and 0.4 according to several tests, because no verified experiment was done in previous.

The second way is to modify the whole CO_2 profile by making its averaged column value equal to SWIR XCO_2. ΔC can be calculated according to the next function and the schematic diagram is shown in Figure 2.3.

$$XCO2\ (SWIR) - XCO2\ (NIES\ TM) = \frac{\sum_{i=1}^{n}(\Delta C_i \times \Delta P_i)}{P_S} \tag{2.11}$$

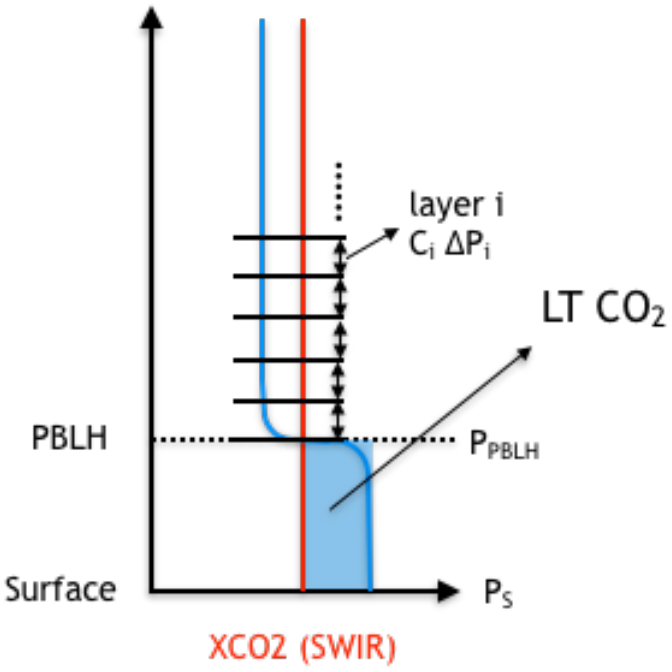

Figure 2.1. Schematic diagram of the method calculating LT CO_2 concentration

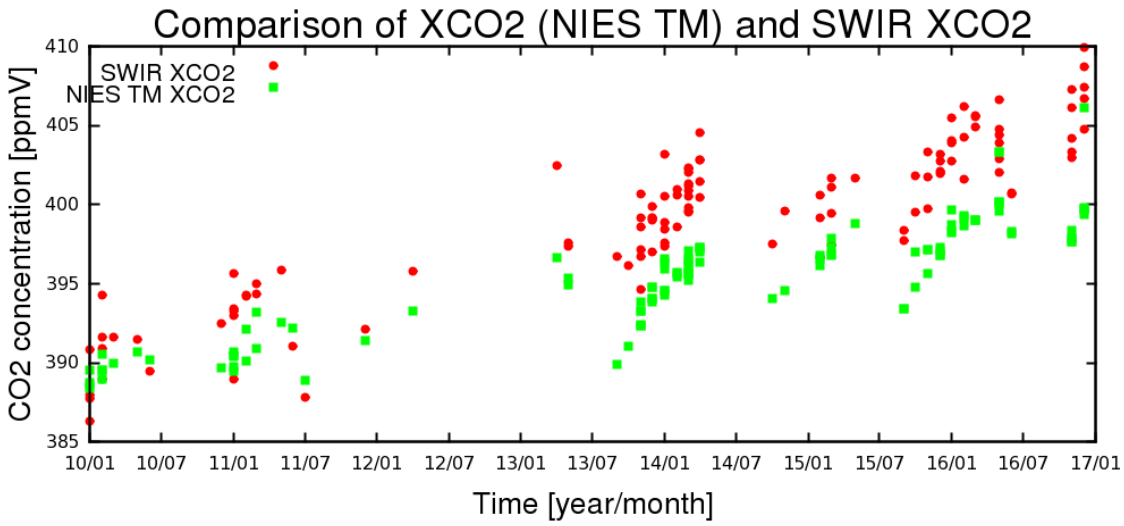

Figure 2.2. Comparing of column averaged value of NIES TM output profile and GOSAT SWIR XCO_2

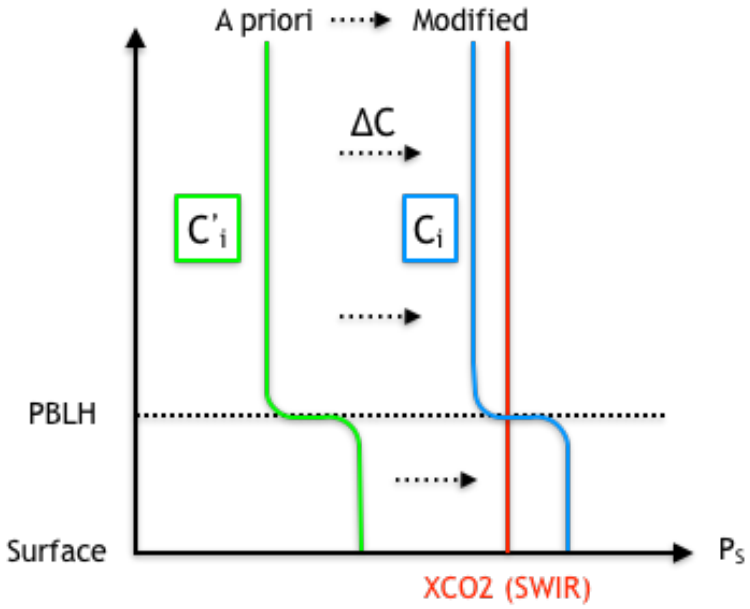

Figure 2.3. Schematic diagram of the second method to modify the CO_2 concentration profiles

Chapter 3

Results and Discussion

The results and discussion are introduced in this chapter and could mainly be divided into three parts: 3.1 mainly describes the performance of temperature retrieval both in simulation and its application over Kanto area from 2010 to 2016 with GOSAT observation; 3.2 is the results about determination of planetary boundary layer height (PBLH) from the retrieved temperature profiles and finally the assessment of calculated lower tropospheric CO_2 concentrations by two different methods and their verification with ground-based observations in Tsukuba city are shown in 3.3.

3.1 Temperature retrieval results

3.1.1 Simulation of retrieving temperature and CO_2

In order to investigate the fundamental performance of the whole retrieval process and the characteristics of thermal infrared radiation, several simulation experiments were carried out using a U.S. standard atmosphere instead before analyzing the real spectrum from GOSAT observation (Rodgers et al., 1998).

Vertical resolution in the retrieval of temperature and CO_2 profiles is one of the superiorities when using TIR spectrum and the superiority could be detected by calculating the Jacobian matrix and the averaging kernel function. Figure 3.1 shows the Jacobian matrix of the atmospheric temperature and CO_2 in 15 μm band from U.S. standard atmosphere, the colour in which represents the sensitivity of the radiance to the variation of atmospheric and surface parameters in each height and each wavenumber. The sensitivity of temperature shows a high value in the middle and upper troposphere from 690 to 740 cm^{-1} and in lower troposphere from 740 to 760 cm^{-1}. Good sensitivity of CO_2 is from 700 to 760 cm^{-1} in around 700hPa. The results demonstrate that the temperature retrieval sensitivity is good in almost all the heights, while CO_2 retrieval sensitivity is better in the middle and upper troposphere than in lower troposphere. The averaging kernel function is shown in Figure 3.2 and the green lines represent AK areas which directly indicates the retrieval sensitivity of temperature and CO_2 profile. The averaging kernel functions were calculated when increasing the temperature profile by 5 Kelvin and CO_2 profile by 1% for each layer, the increased value also contributed to the diagonal

elements in the a priori covariance matrix. The results indicate a higher effectiveness from 900hPa to 40hPa for temperature retrieval and 600-200hPa for CO_2 retrieval.

The sensitivity in CO_2 retrieval is different between upper and lower troposphere, mainly on account of the influence of the surface skin temperature. This characteristic resulted in further researches on the averaging kernel function variation when surface skin temperature changes. The results of CO_2 averaging kernel function when increasing the surface skin temperature by 5 Kelvin and 10 Kelvin are shown in Figure 3.3. An apparent increasing feature could be seen in the lower troposphere. When the surface skin temperature increases, the sensitivity of CO_2 retrieval in lower troposphere also becomes larger, which provides a possibility of retrieving lower tropospheric CO_2 concentration when surface skin temperature is high.

3.1.2 Temperature retrieval over Kanto area

With a good sensitivity in almost all the heights, temperature including surface skin temperature and atmospheric temperature profiles over Kanto area were retrieved simultaneously using the spectrum data from GOSAT, all the retrieved results are implemented under the condition with a clear sky. To evaluate the bias and the precisions in the retrieved temperature profiles, temperature profiles from radiosonde measurement in Tsukuba were used to compare with. The radiosonde profiles are smoothed by the TANSO-FTS averaging kernels according to Equation (3.1)

$$\hat{x}_{sonde} = x_a + A(x_{sonde} - x_a) \tag{3.1}$$

where $\hat{\boldsymbol{x}}_{\boldsymbol{sonde}}$ and $\boldsymbol{x_{sonde}}$ are the smoothed and original radiosonde profiles, respectively. $\boldsymbol{x_a}$ is the output profile data from the numerical simulation of NIES TM (Ohayama et al., 2013). Figure 3.4 shows the difference of the TANSO-FTS temperature profile retrievals from the radiosonde measurements during the observation and about 416 data points were matched for 5 years from 2009 to 2014. The comparison has the mean differences within 2K and a standard deviation of ±2K. A larger difference and standard deviation observed in the lower troposphere are mainly due to the time differences between the data sets are almost around 4 hours. The bias in upper troposphere may be introduced by uncertainties in the L1B calibration processing (Kuze et al., 2012).

Originally, the retrieval of CO_2 profile from TIR spectra should have been one of the most important parts in this study, meanwhile, the significance of surface skin temperature is mentioned in 3.1 that high surface skin temperature will increase the sensitivity in the lower tropospheric CO_2 retrieval, so the surface skin temperature was chosen to be the key study object. Also, higher heat contrast due to heat island effect in megacity also provides the reason of choosing Kanto area in Japan

to be studied here. The results shown in Figure 3.5 are the averaged annual variation of surface skin temperature from 2010 to 2016 over Kanto area. All the observation data is averaged into a 0.1°×0.1° grid. The cloud cover in summer is more than that in winter, which makes the observation points in summer become fewer. From the results, an apparent variation can be detected that the surface skin temperature is higher in July and August with the highest value of 322K; and lower in December and January with the lowest value of 275K. Because the surface skin temperature is largely influenced by the thermal radiation and landform, it usually is higher than the atmospheric temperature near surface. From the results, the observed surface skin temperatures also appear to be different between urban and rural area, for the different surfaces: concrete in urban and asphalt in rural. In order to detect the time series variation of surface skin temperature and temperature profile during the observation period, further study was implemented to focus on Tsukuba and Tokyo city, the results of which are shown in Figure 3.6. The spatial matchup in two cities are both within 100km from the central area and it is lack of data for different meteorological conditions. The plots of surface skin temperature and temperature profiles in Tsukuba and Tokyo both show an obvious variation in each year that high in summer and low in winter. Compared to Tsukuba, the temperature profile in Tokyo has less regularity and stability, may due to a stronger influence from heat island or other meteorological conditions. Also, the surface skin temperature in Tokyo appears to be higher than that in Tsukuba city, which may be owing to a higher bustling level in Tokyo.

3.2 Determination of planetary boundary layer height

PBLH in the path time of GOSAT (local time 13:15) over Kanto area is estimated by using the vertical gradient of the potential temperature profile, which is transformed from the retrieved atmospheric temperature profile. The profile includes around 7 levels within 4km above the mean sea level. In order to decrease the possibility of mistaking with free tropospheric features, estimated PBLH that exceeds 4000m above the surface is not considered. Figure 3.7 shows the time series variations of potential temperature in Tsukuba and Tokyo and the black triangle in the figure represents the height of determined PBL. The results show a relatively vague trend that the PBLH becomes lower in summer and higher in winter, which mainly owing to the influence from surface thermal activity and several meteorological factors.

In order to perform an accurate estimation, estimated PBLH by retrieved potential temperature profile from GOSAT is compared with that from radiosonde measurements. A comparison is performed with the PBLH from radiosonde profiles in Tsukuba city, the distance is within 50km. Figure 3.8 shows the PBLH comparison between GOSAT and radiosonde profiles using potential temperature profiles, the x and y axis of which are expressed in pressure (hPa). The number of

atmospheric observation level in radiosonde below 4km is about 12, which represents a higher vertical resolution in radiosonde profile. The result illustrates that PBLH from GOSAT has a agreement with that from radiosonde profiles with a coefficient of determination (R^2) 0.40137. The time differences that radiosonde measurements are earlier than that of GOSAT should have been reflected with a lower height of PBL in radiosonde measurements in the comparison, the underestimation of PBLH with GOSAT could be mainly due to the low vertical resolution.

3.3 Results of lower tropospheric CO_2 concentration

Lower tropospheric CO_2 concentrations are calculated in the synergy of SWIR XCO_2 and CO_2 profiles, based on the determination of PBLH. The detailed information of the calculation is introduced in 2.4. Ground-based observation data from the meteorological tower and in situ measurements by AIST in Tsukuba are used in this step to verify the accuracy and precision of the estimated lower tropospheric CO_2 concentration. The ground-based observation data is first used to be compared with GOSAT SWIR XCO_2 and the result is shown in Figure 3.9. About 77 data sets are matched, the distance of which is within 50km and the time differences of which are within one hour. Most of the SWIR XCO_2 data points appear to be lower than the concentration of ground-based observation in the graph. The underestimation of SWIR XCO_2 could come down to its low sensitivity to local surface fluxes, which also states that the lower tropospheric CO_2 concentration can reflect more information about the surface fluxes.

As mentioned above, there are three parameters need to be determined to estimate LT CO_2 concentration: (1) XCO_2; (2) PBLH; (3) upper-air concentration from the CO_2 profile. The CO_2 profiles can be obtained either from the output of NIES TM or GOSAT TIR L2 standard product, but the accuracy of these two profiles are both worth of more discussion. In this step, two sources profiles are both used to estimate the LT CO_2 concentration and the results of them are also divided into two parts to be introduced: using numerical simulation CO_2 profile from NIES TM and CO_2 profile from GOSAT TIR L2 standard product.

3.3.1 Numerical simulation profile

Because the value of the growth rate of CO_2 in NIES TM was underestimated, the output CO_2 profiles have to be modified before calculating the LT CO_2 concentration, two modifier methods: (1) modify according to time difference ($LTCO_2$ TD) and (2) modify according to the value of SWIR XCO_2 ($LTCO_2$ SX) are used, the detail is introduced in 2.4.

In the atmosphere, the mixing motions typically engulf the lowest 1 to 2km when convection occurs. So, the planetary boundary layer is first set to 850hPa (about 1.5km above the mean sea level),

in order to simplify the whole calculating process and prove good results can be obtained by the modified CO_2 profiles.

(a) PBLH assumed to be 850hPa

LT CO_2 concentrations including $LTCO_2$ TD and $LTCO_2$ SX are calculated using modified CO_2 profiles with two different methods. The comparison results with ground-based observation are shown in Figure 3.10, the x and y axis ranges of which are the same. The GOSAT SWIR XCO_2 data are also plotted in Figure 3.10 as a reference to show the improvement. Compared to SWIR XCO_2, $LTCO_2$ TD and $LTCO_2$ SX both show better results that the data points are much closer to the ground-based observation. Also, compared to $LTCO_2$ TD, LT CO_2 SX from the second method shows a better result that the data points appear to be more concentrated and a better correlation.

(b) PBLH determined by retrieving potential temperature profile

Based on the good result when assuming the PBLH to be 850hPa, these two methods are also both applied to the realistic condition that PBLH is determined from retrieved temperature profile. The results are shown in Figure 3.11. The data points are less than that in Figure 3.10 because there are many cases that PBLH cannot be determined. They still appear to have a better result than SWIR XCO_2, but compared to $LTCO_2$ TD, a better result could be found in $LTCO_2$ SX obviously.

In order to compare the results further and get more detailed information, each data point is further researched and the quantitative analysis result is shown in Table 3.1. The "STD" means the standard deviation and all the data are calculated by taking the difference from ground-based observation. In both situations, the calculated LT CO_2 concentration by two different methods both have a much smaller mean value of difference than that of SWIR XCO_2, which states the superiority of estimating LT CO_2 concentration. The $LTCO_2$ SX shows a smaller STD of difference and higher R-square value in both situations than that of SWIR XCO_2 and $LTCO_2$ TD, which proves that the second method ($LTCO_2$ SX) is more suitable for calculating LT CO_2 concentration. Also, it is found that when $LTCO_2$ SX is applied to the realistic condition, the value of STD for $LTCO_2$ SX changes from 3.964 to 2.902 while the R-square still keeps the same level, which states a good practicability and a superiority of this method presented here.

Table 3.1. Detailed information about the LT CO_2 concentration using numerical simulation profiles

	SWIR XCO_2	LT CO_2 TD	LT CO_2 SX
PBLH assumed to 850hPa			
Number of data	77	77	77
Mean value of diff. [ppmv]	9.029	1.903	1.773
STD of diff. [ppmv]	5.068	6.702	3.964
R-square	0.568	0.418	0.743
PBLH determined from retrieved potential temperature profile			
Number of data	15	15	15
Mean value of diff. [ppmv]	7.753	0.372	2.594
STD of diff. [ppmv]	3.529	6.106	2.902
R-square	0.580	0.163	0.709

3.3.2 TIR L2 profile

After the lower tropospheric CO_2 concentration is estimated by using the numerical simulation output CO_2 profile above, LT CO_2 concentration is also estimated by the GOSAT TIR L2 profile here, which could be downloaded from the official website as a standard product. LT CO_2 concentration is also estimated under two situations: PBLH is assumed to be 850hPa and determined from retrieved temperature profiles. The results are shown in Figure 3.12. The two graphs both show quite scattering results and the detailed information is listed in Table 3.2. The two results in two situations both have big minus mean values and large standard deviations, which both exceed 15 ppmv. Based on the calculation function, the overestimation of the LT CO_2 concentration should be due to low concentration in upper air. Saitoh et al (2017) assessed the bias of lower and middle tropospheric CO_2 concentration of GOSAT TIR standard product and states that large negative biases exist in the lower and middle tropospheric regions. The part of the reason was the absorption bands in the retrieval algorithm. The accuracy of the CO_2 profile from GOSAT TIR standard product is expected to be much better for GOSAT-2 sensors because the signal to noise ratio (SNR) of the new sensor and systematic biases of radiance measurement will be drastically improved.

Table 3.2. Detailed information about the LT CO_2 concentration using TIR L2 product

	LT CO_2 TIR L2
PBLH assumed to 850hPa	
Number of data	31
Mean value of diff. [ppmv]	-18.043
STD of diff. [ppmv]	17.860
R-square	0.475
PBLH determined from retrieved potential temperature profile	
Number of data	4
Mean value of diff. [ppmv]	-22.723
STD of diff. [ppmv]	15.057
R-square	0.680

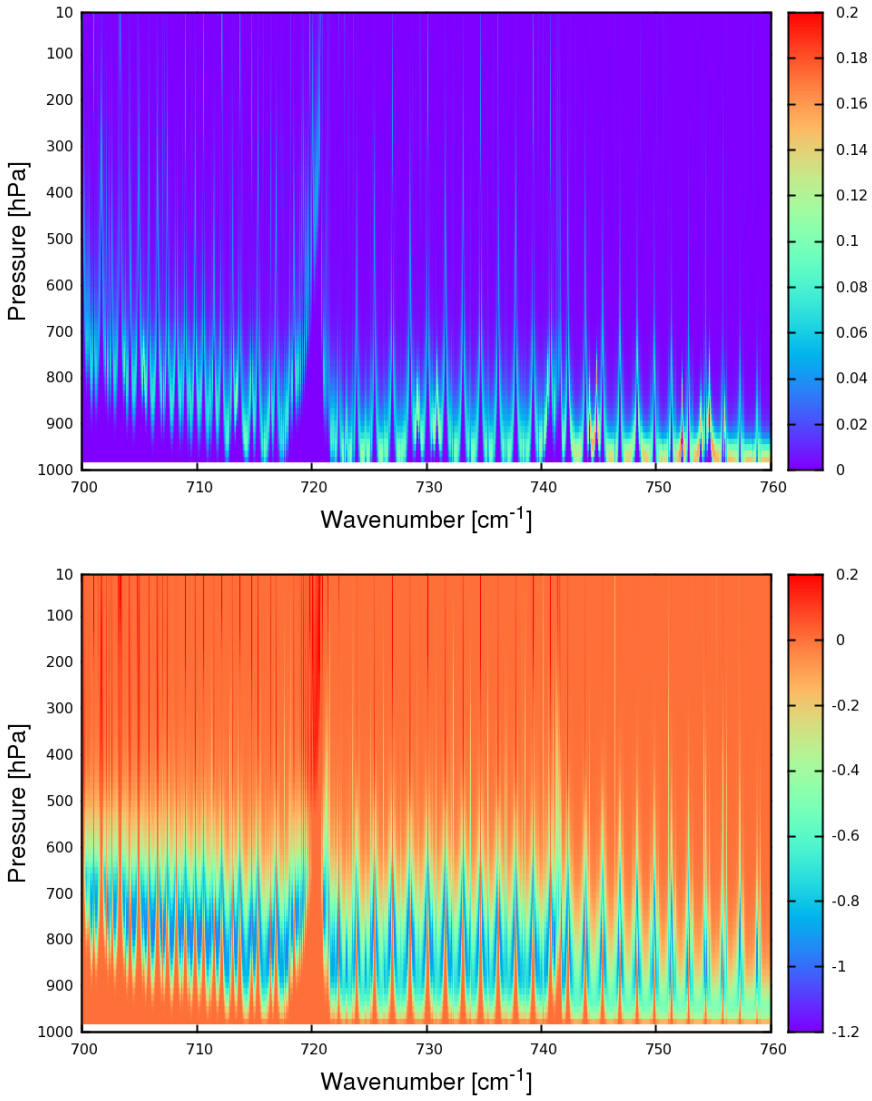

Figure 3.1. Example of temperature (upper) and CO_2 (lower) Jacobian matrix using U.S. standard atmosphere

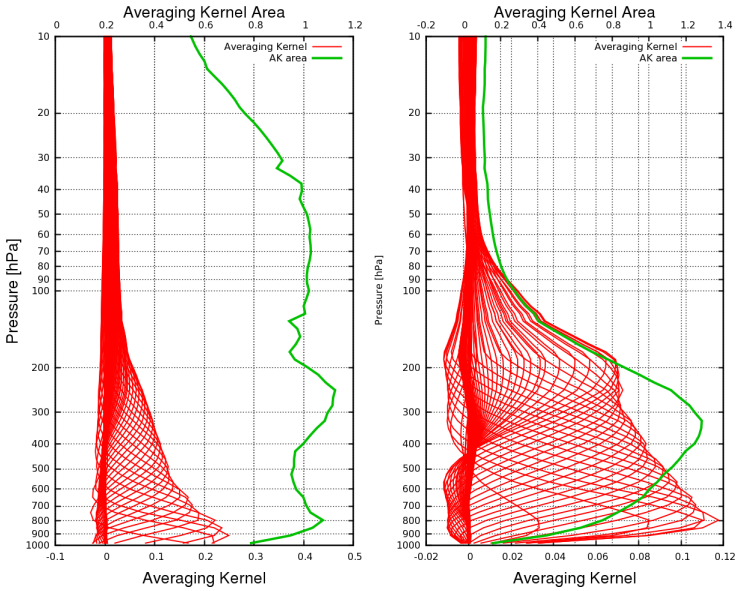

Figure 3.2. Averaging kernel function of temperature (left) and CO_2 (right) retrieval and the green lines in these two graphs both represent AK areas.

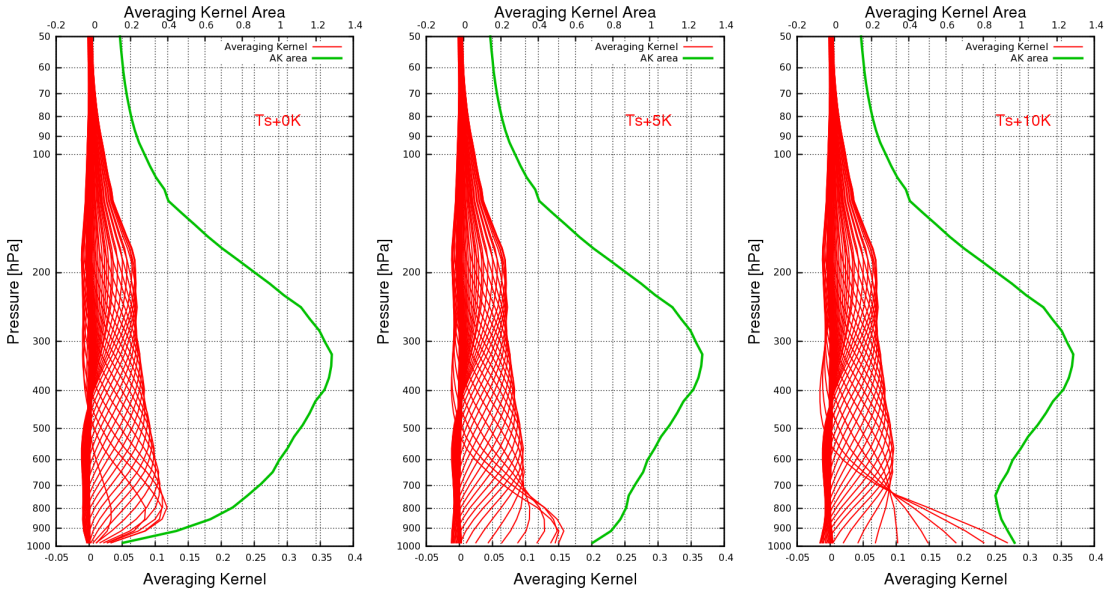

Figure 3.3. Averaging kernel function of CO_2 retrieval when increasing surface skin temperature by 5, 10 Kelvin at a U.S. standard atmosphere. The green lines in these two graphs both represent AK areas.

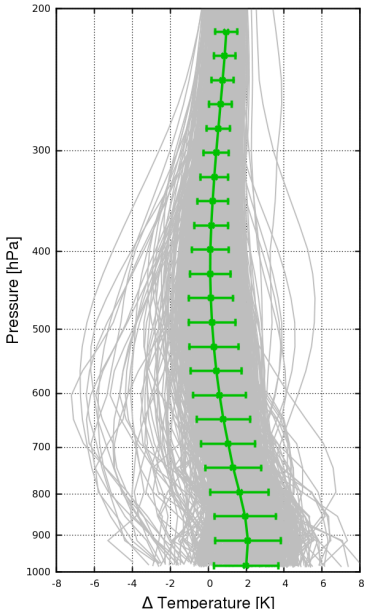

Figure 3.4. Temperature differences of TANSO-FTS retrievals from the radiosonde measurements in Tsukuba. The grey solid lines denote all the individual comparisons and the green solid line and error bars represent the mean differences and standard deviations, respectively.

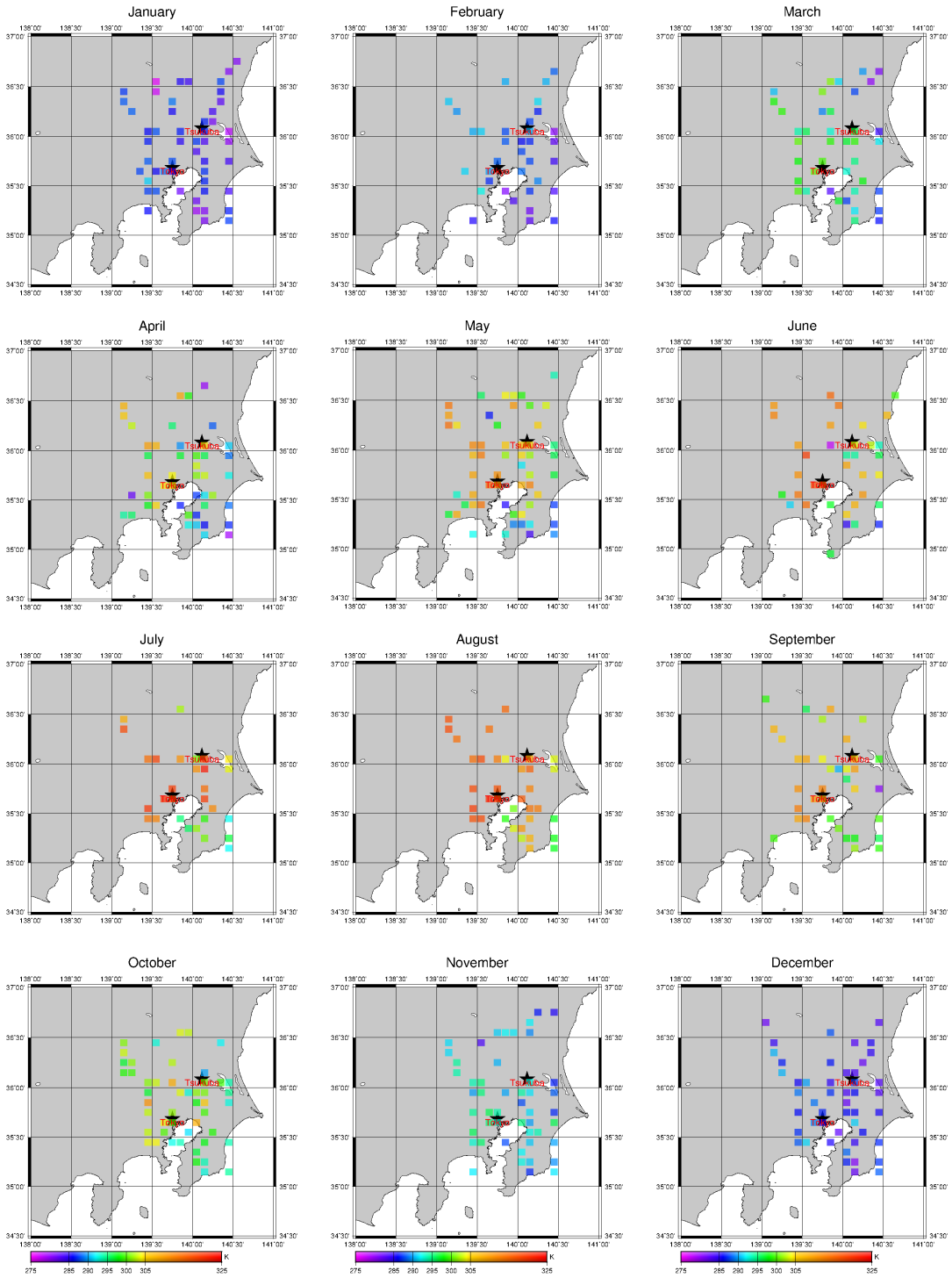

Figure 3.5. Averaged annual variation of surface skin temperature in around 13:00 from 2010 to 2016 over Kanto area, Japan. The color bar in each graph keeps the same.

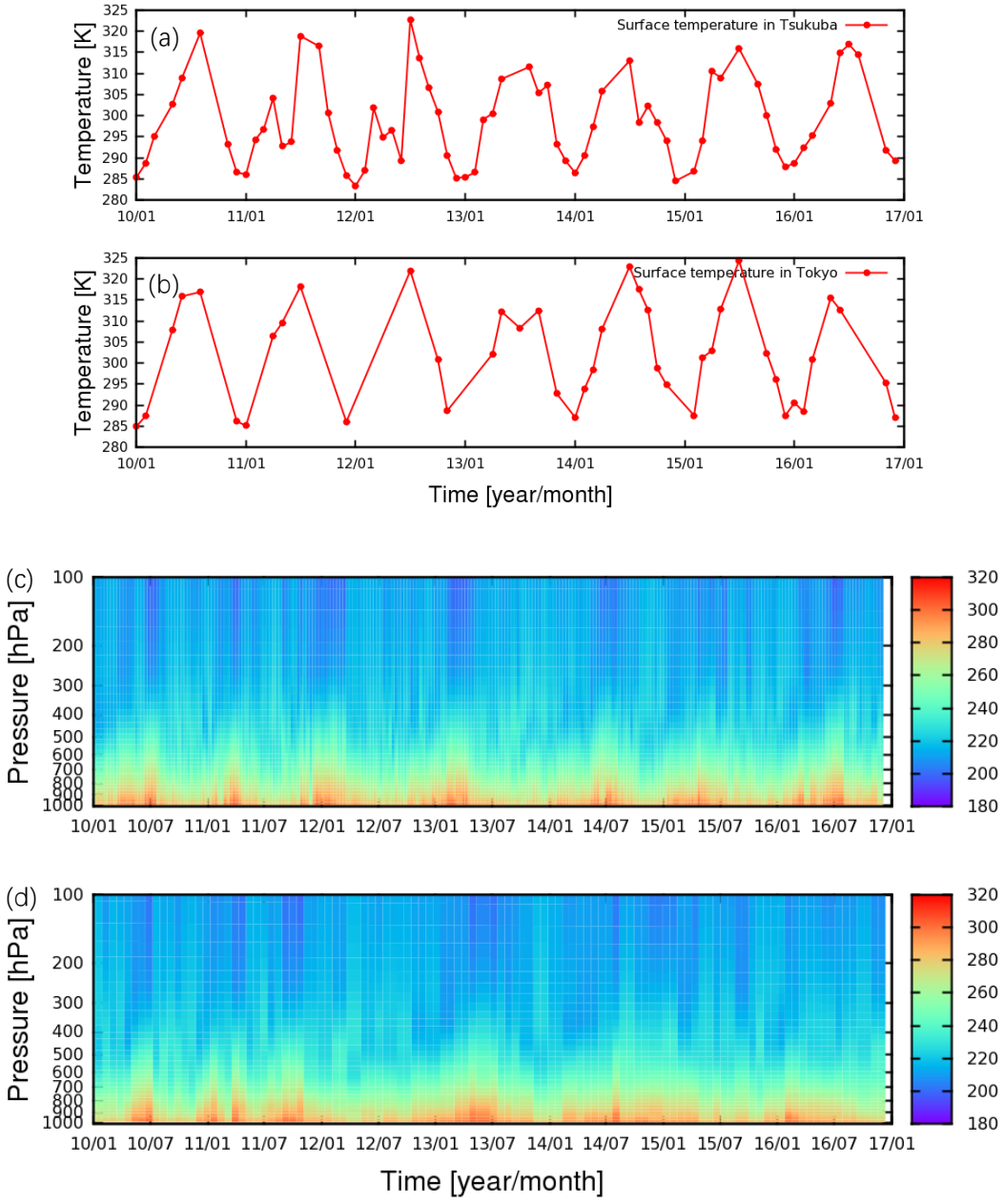

Figure 3.6. Time series data of surface skin temperature in Tsukuba (a) and Tokyo (b) city; atmospheric temperature profile in Tsukuba (c) and Tokyo (d) city from 2010 to 2016.

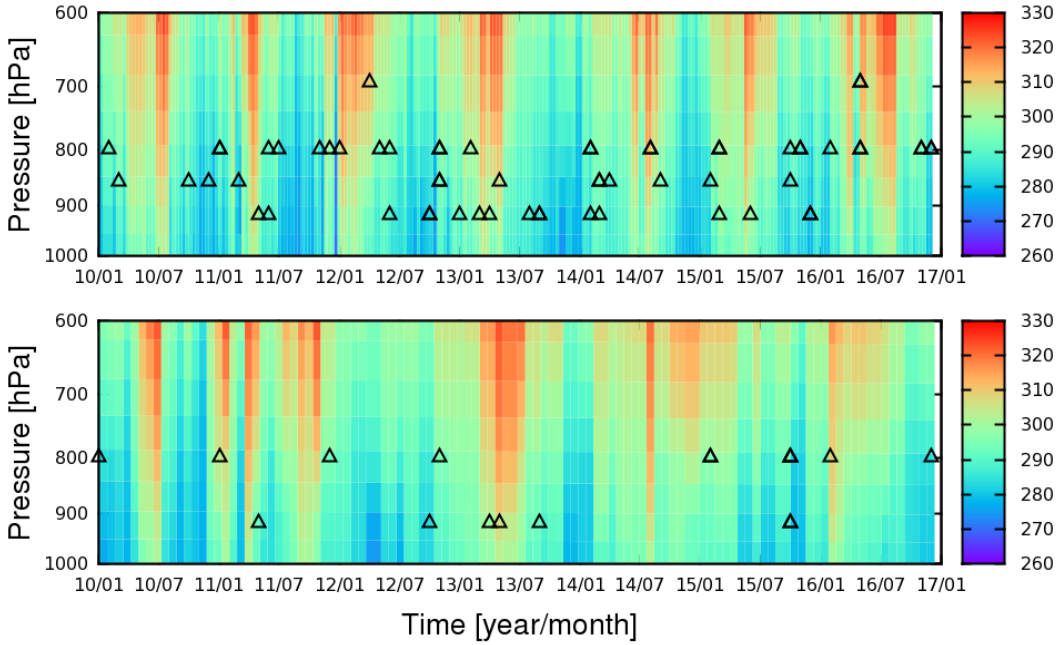

Figure 3.7. Time series of potential temperature profile in Tsukuba (upper) and Tokyo (lower), the black triangle denote the determined PBLH.

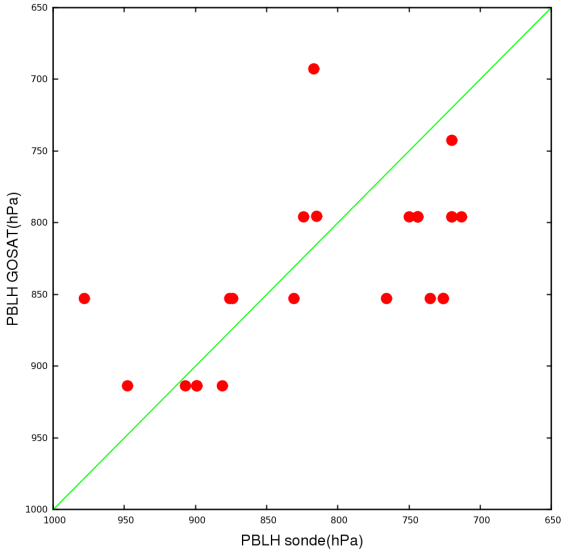

Figure 3.8. The comparison of PBLH between radiosonde measurements and GOSAT observation, the unity of PBLH is shown in pressure.

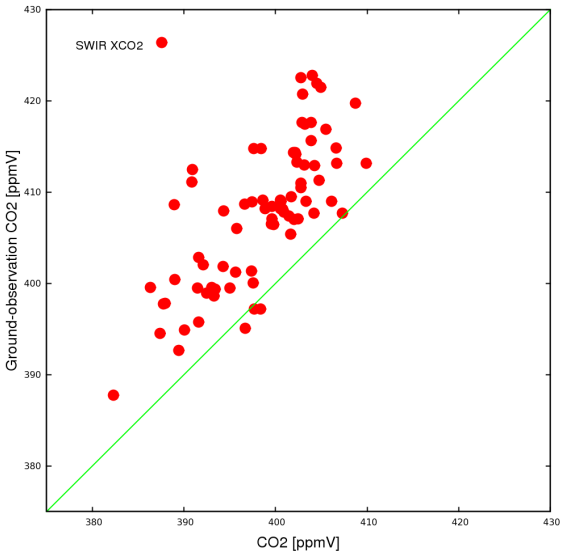

Figure 3.9. The comparison of GOSAT SWIR XCO_2 and ground-based observation in Tsukuba.

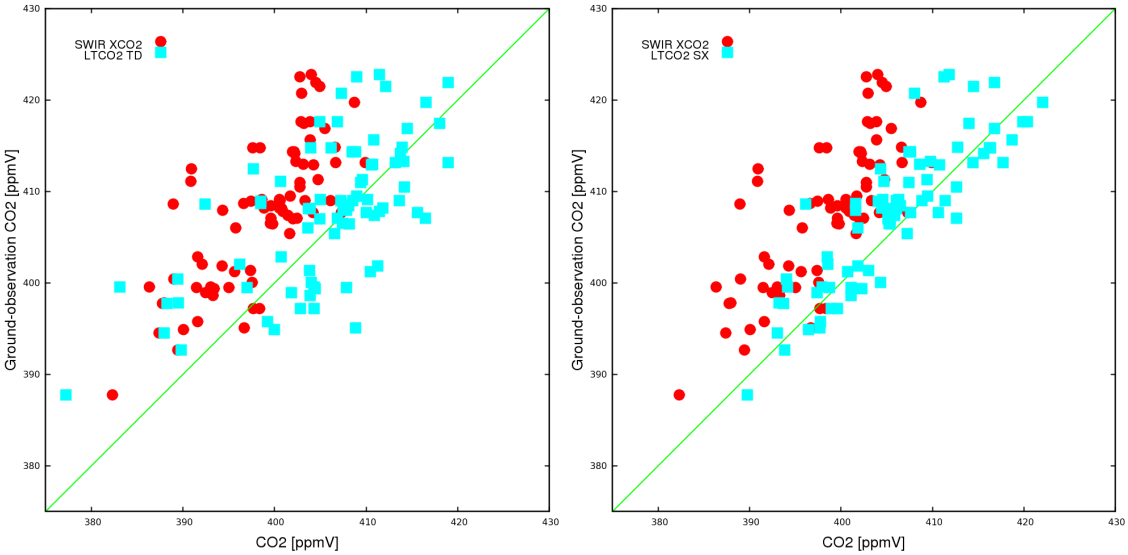

Figure 3.10. Comparison between LT CO_2 concentration and ground-based observation in Tsukuba, when assuming PBLH to be 850hPa. LT CO_2 are calculated in two different methods: $LTCO_2$ TD (left) and $LTCO_2$ SX (right)

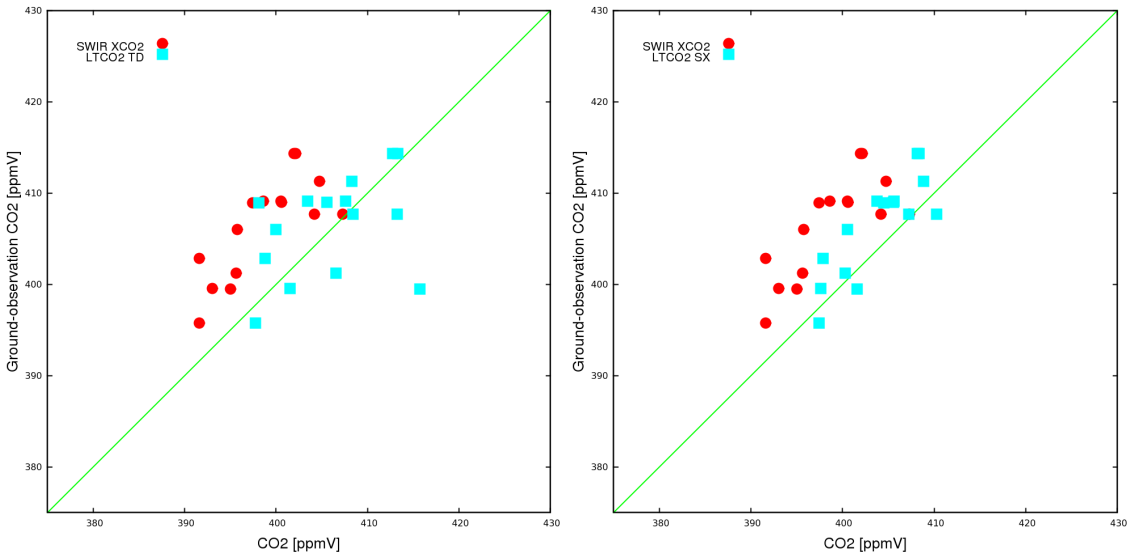

Figure 3.11. Comparison between LT CO_2 concentration and ground-based observation in Tsukuba, when PBLH is retrieved from GOSAT temperature profile. LT CO_2 are calculated in two different methods: $LTCO_2$ TD (left) and $LTCO_2$ SX (right)

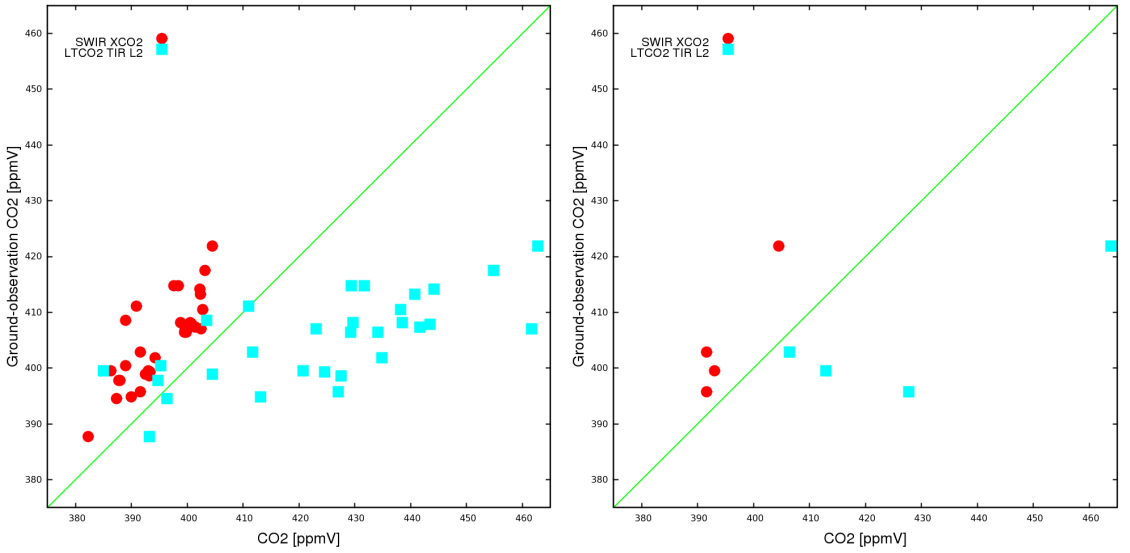

Figure 3.12. Comparison results of ground-based observation and estimated LT CO_2 using TIR L2 product when PBLH is assumed to 850hPa (left) and determined from retrieved temperature profile (right).

Chapter 4

Summary and Conclusion remarks

The total column concentration of CO_2 is partly driven by local surface fluxes which makes the estimation of near-surface CO_2 concentration become more important in the determination of sources and sinks. The CO_2 concentration below PBL (lower troposphere, LT) is estimated in the synergy of GOSAT SWIR XCO_2 and upper-air CO_2 profile. Upper-air CO_2 profile comes from two different sources. Also, the accuracy and precision of the estimated LT CO_2 concentration are examined in this study.

PBLH is determined from temperature profile, so firstly the surface skin temperature and temperature profile over Kanto area from 2010 to 2016 are retrieved from GOSAT spectrum. Radiosonde profiles obtained in Tsukuba are used to verify the accuracy of the retrieved temperature profiles. The mean difference between retrieved temperature profiles and radiosonde observation is less than 2K and the mean standard deviation is ±2K. The maximum value exists in lower troposphere, which can be accepted for the 4 hours difference between GOSAT and radiosonde observation. The variation of retrieved surface skin temperature shows an obvious change during a year that high in summer and low in winter and also an apparent difference could be observed between the urban and rural area.

Determination of PBLH as the altitudes of the maximum vertical gradient of potential temperature is followed in the study. PBLH estimated from retrieved potential temperature profiles shows a reasonable correlation with that being estimated using radiosonde measurements.

By synergetic usage of SWIR XCO_2 and upper-air CO_2 profile, LT CO_2 concentration in PBL is estimated. Two types of CO_2 profile are used in this research. The CO_2 profile outputted from numerical simulation (by use of NIES TM) is used firstly. The relatively low setting of CO_2 growth rate in the NIES TM make the value of output CO_2 profile lower than the actual value. Two modifier approaches are applied to modify the output CO_2 profile: (1) modify the CO_2 profile above PBLH according to the time difference since launch of GOSAT; (2) modify the CO_2 profile above PBLH by making the column concentration of CO_2 profile equal to the value of SWIR XCO_2. Compared to SWIR XCO_2, the estimated LT CO_2 concentration from those two methods both show better agreement with the ground-based observation when PBLH is assumed to be 850hPa. The mean value

of difference of estimated LT CO_2 from ground-based observation are lower than 2 ppmv for both methods and the LT CO_2 concentration from the second method has a lower STD compared to that from the first method. Then the two approaches are applied to the realistic condition that PBLH is determined from retrieved temperature profile. The estimated LT CO_2 concentration from the second method still shows a lowest mean value of difference. Also, when applied to the realistic condition, the STD of the estimated LT CO_2 of the second method becomes smaller, changing from 3.964 to 2.902 (ppmv), which illustrates a good practicability and a superiority of the second method presented here. As the final approach, the CO_2 profile from GOSAT TIR L2 standard product is used for estimating LT CO_2 concentration. The comparison with ground-based observations shows a quite scatter result in both situations of PBLH. Considering the results from the comparison, an underestimation in the upper-air CO_2 concentration could be concluded. The accuracy of the CO_2 profile from GOSAT TIR L2 standard product is expected to be much better for GOSAT-2 sensors because the signal to noise ratio (SNR) of the new sensor and systematic biases of radiance measurement will be drastically improved.

Above all, this study provides an effective approach of estimating LT CO_2 concentration with synergetic usage of the modified output CO_2 profile from NIES TM and GOSAT SWIR XCO_2. Meanwhile, the weakness of using TIR L2 product is pointed out and improved CO_2 profile is expected in GOSAT-2 project. These conclusions can contribute to the further study of estimating LT CO_2 concentration.

References

[1] Baker, D. F., Bosch, H., Doney, S. C., O'Brien, D., & Schimel, D. S. (2010). Carbon source/sink information provided by column CO_2 measurements from the Orbiting Carbon Observatory.

[2] Chevallier, F., Engelen, R. J., & Peylin, P. (2005). The contribution of AIRS data to the estimation of CO_2 sources and sinks. Geophysical Research Letters, 32(23).

[3] Christi, M. J., & Stephens, G. L. (2004). Retrieving profiles of atmospheric CO_2 in clear sky and in the presence of thin cloud using spectroscopy from the near and thermal infrared: A preliminary case study. Journal of Geophysical Research: Atmospheres, 109(D4).

[4] Clough, S. A., Iacono, M. J., & Moncet, J. L. (1992). Line- by- line calculations of atmospheric fluxes and cooling rates: Application to water vapor. Journal of Geophysical Research: Atmospheres, 97(D14), 15761-15785.

[5] Clough, S. A., Shephard, M. W., Mlawer, E. J., Delamere, J. S., Iacono, M. J., Cady-Pereira, K., & Brown, P. D. (2005). Atmospheric radiative transfer modeling: a summary of the AER codes. Journal of Quantitative Spectroscopy and Radiative Transfer, 91(2), 233-244.

[6] Griffith, D. W., Toon, G. C., Connor, B., Sussmann, R., Warneke, T., Deutscher, N. M., Wennberg, P. O., Notholt, J., Sherlock, V., Robinson, J., Uchino, O., Roehl, C. M., Morino, I., Wunch, D., Messerschmidt, J., Yoshida, Y., Inoue, M., & Rettinger, M. (2011). Preliminary validation of column-averaged volume mixing ratios of carbon dioxide and methane retrieved from GOSAT short-wavelength infrared spectra. Atmospheric Measurement Techniques, 4 (6), 1061-1076.

[7] Han, Y., Revercomb, H., Cromp, M., Gu, D., Johnson, D., Mooney, D., Scott, D., Strow, L., Bingham, G., Borg, L., Chen, Y., DeSlover, D., Esplin, M., Hagan, D., Jin, X., Knuteson, R., Motteler, H., Predina, J., Suwinski, L., Talyor, J., Tobin, D., Tremblay, D., Wang, C., Wang, L., Wang, L., & Zavyalov, V. (2013). Suomi NPP CrIS measurements, sensor data record algorithm, calibration and validation activities, and record data quality. Journal of Geophysical Research: Atmospheres, 118(22).

[8] Hennemuth, B., & Lammert, A. (2006). Determination of the atmospheric boundary layer height from radiosonde and lidar backscatter. Boundary-Layer Meteorology, 120(1), 181-200.

[9] Inoue, M., Morino, I., Uchino, O., Miyamoto, Y., Yoshida, Y., Yokota, T., Machida, T., Sawa, Y., Matsueda, H., Sweeney, C., Tans, P. P., Andrews, A. E., Biraud, S. C., Tanaka, T., Kawakami, S., & Patra, P. K. (2013). Validation of XCO 2 derived from SWIR spectra of GOSAT TANSO-FTS with aircraft measurement data. Atmospheric Chemistry and Physics, 13(19), 9771-9788.

[10] Iwasaki, C., Imasu, R., Bril, A., Yokota, T., Yoshida, Y., Morino, I., Oshchepkov, S., Wunch, D., Griffith, D. W. T., Deutscher, N. M., Kivi, R., Pollard, D., Roehl, C. M., Velazco, V. A., Sussmann, R., Warneke, T., & Notholt, J. (2017). Validation of GOSAT SWIR XCO2 and XCH4 Retrieved by PPDF-S Method and Comparison with Full Physics Method. SOLA, 13, 168-173.

[11] Keppel-Aleks, G., Wennberg, P. O., & Schneider, T. (2011). Sources of variations in total column carbon dioxide. Atmospheric Chemistry and Physics, 11(8), 3581-3593.

[12] Kuze, A., Suto, H., Shiomi, K., Urabe, T., Nakajima, M., Yoshida, J., Kawashima, T., Tamamoto, Y., Kataoka, F., & Buijs, H. (2012). Level 1 algorithms for TANSO on GOSAT: processing and on-orbit calibrations. Atmospheric Measurement Techniques, 5(10), 2447.

[13] Liu, Y., Yang, D., & Cai, Z. (2013). A retrieval algorithm for TanSat XCO 2 observation: Retrieval experiments using GOSAT data. Chinese Science Bulletin, 58(13), 1520-1523.

[14] Maddy, E. S., Barnet, C. D., Goldberg, M., Sweeney, C., & Liu, X. (2008). CO_2 retrievals from the Atmospheric Infrared Sounder: Methodology and validation. Journal of Geophysical Research: Atmospheres, 113(D11).

[15] Maddy, E. S., Barnet, C. D., Goldberg, M., Sweeney, C., & Liu, X. (2008). CO_2 retrievals from the Atmospheric Infrared Sounder: Methodology and validation. Journal of Geophysical Research: Atmospheres, 113(D11).

[16] Maksyutov, S., Patra, P. K., Onishi, R., Saeki, T., & Nakazawa, T. (2008). NIES/FRCGC global atmospheric tracer transport model: description, validation, and surface sources and sinks inversion, J. Earth Simulator, 9, 3-18.

[17] Maksyutov, S., Takagi, H., Valsala, V. K., Saito, M., Oda, T., Saeki, T., Belikov, D. A., Saito, A., Yoshida, Y., Morino, I., Uchino, O., Andres, R. J., & Yokota, T. (2013). Regional CO_2 flux estimates for 2009-2010 based on GOSAT and ground-based CO_2 observations. Atmospheric Chemistry and Physics, 13(18), 9351-9373.

[18] Ohyama, H., Kawakami, S., Shiomi, K., Morino, I., & Uchino, O. (2013). Atmospheric temperature and water vapor retrievals from GOSAT thermal infrared spectra and initial validation with coincident radiosonde measurements. SOLA, 9, 143-147.

[19] Pachauri, R. K. , Allen, M. R. , Barros, V. R. , Broome, J. , Cramer, W. , Christ, R. , Church, J. A. , Clarke, L. , Dahe, Q. , Dasgupta, P. , Dubash, N. K. , Edenhofer, O. , Elgizouli, I. , Field, C.

B. , Forster, P. , Friedlingstein, P. , Fuglestvedt, J. , Gomez-Echeverri, L. , Hallegatte, S. , Hegerl, G. , Howden, M. , Jiang, K. , Jimenez Cisneroz, B. , Kattsov, V. , Lee, H. , Mach, K. J. , Marotzke, J. , Mastrandrea, M. D. , Meyer, L. , Minx, J. , Mulugetta, Y. , O'Brien, K. , Oppenheimer, M. , Pereira, J. J. , Pichs-Madruga, R. , Plattner, G. K. , Pörtner, H. O. , Power, S. B. , Preston, B. , Ravindranath, N. H. , Reisinger, A. , Riahi, K. , Rusticucci, M. , Scholes, R. , Seyboth, K. , Sokona, Y. , Stavins, R. , Stocker, T. F. , Tschakert, P. , van Vuuren, D. and van Ypserle, J. P. (2014). Climate change 2014: synthesis report. Contribution of Working Groups I, II and III to the fifth assessment report of the Intergovernmental Panel on Climate Change (p. 151). IPCC.

[20] Rodgers, C. D. (2000). Inverse methods for atmospheric sounding: theory and practice (Vol. 2). World scientific.

[21] Rodgers, C. D. (1996, October). Information content and optimization of high-spectral-resolution measurements. In Optical spectroscopic techniques and instrumentation for atmospheric and space research II (Vol. 2830, pp. 136-148). International Society for Optics and Photonics.

[22] Prijith, S. S., Rao, P. V. N., Sujatha, P., & Dadhwal, V. K. (2016). Estimation of planetary boundary layer height using Suomi NPP-CrIS soundings. Remote Sensing Letters, 7(7), 621-630.

[23] Saitoh, N., Imasu, R., Ota, Y., & Niwa, Y. (2009). CO_2 retrieval algorithm for the thermal infrared spectra of the Greenhouse Gases Observing Satellite: Potential of retrieving CO_2 vertical profile from high-resolution FTS sensor. Journal of Geophysical Research: Atmospheres, 114(D17).

[24] Saitoh, N., Kimoto, S., Sugimura, R., Imasu, R., Kawakami, S., Shiomi, K., ... & Matsueda, H. (2016). Algorithm update of the GOSAT/TANSO-FTS thermal infrared CO_2 product (version 1) and validation of the UTLS CO_2 data using CONTRAIL measurements. Atmospheric Measurement Techniques, 9(5), 2119-2134.

[25] Saitoh, N., Kimoto, S., Sugimura, R., Imasu, R., Shiomi, K., Kuze, A., Machida, T., Sawa, Y., & Matsueda, H. (2017). Bias assessment of lower and middle tropospheric CO 2 concentrations of GOSAT/TANSO-FTS TIR version 1 product. Atmospheric Measurement Techniques, 10(10), 3877.

[26] Stephens, B. B., Gurney, K. R., Tans, P. P., Sweeney, C., Peters, W., Bruhwiler, L., Ciais, P., Ramonet, M., Bousquet, P., Nakazawa, T., Aoki, S., Machida, T., Inoue, G., Vinnichenko, N., Lloyd, J., Jordan, A., Heimann, M., Shibistova, O., Langenfelds, R. L., Steele, L. P., Francey, R. J., & Denning, A. S. (2007). Weak northern and strong tropical land carbon uptake from vertical profiles of atmospheric CO_2. Science, 316(5832), 1732-1735.

[27] Stull, R. B. (2012). An introduction to boundary layer meteorology (Vol. 13). Springer Science & Business Media.

[28] Takagi, H., Houweling, S., Andres, R. J., Belikov, D., Bril, A., Boesch, H., Butz, A., Guerlet, S., Hasekamp, O., Maksyutov, S., Morino, I., Oda, T., O'Dell, C. W., Oshchepkov, S., Parker, R., Saito, M., Uchino, O., Yokota, T., Yoshida, Y., & Valsala, V. (2014). Influence of differences in current GOSAT XCO_2 retrievals on surface flux estimation. Geophysical Research Letters, 41(7), 2598-2605.

[29] XY Wang, & KC Wang (2014). Estimation of atmospheric mixing layer height from radiosonde data. Atmospheric Measurement Techniques, 7(6), 1701-1709.

[30] Yokota, T., Oguma, H., Morino, I., Higurashi, A., Aoki, T., & Inoue, G. (2004, November). Test measurements by a BBM of the nadir-looking SWIR FTS aboard GOSAT to monitor CO_2 column density from space. In Proc. of SPIE Vol (Vol. 5652, p. 183)

Acknowledgement

Foremost, I would like to express my sincere appreciation to my advisor Prof. Imasu for the continuous support of my master study and research, for his patience, motivation, enthusiasm, and immense knowledge. Although I was a starter in this field, his guidance did help me in all the time of research and writing of this thesis. I could not have imagined having a better advisor and mentor for my master study.

Besides my advisor, my sincere thanks also goes to Dr. Someya and Dr. Iwasaki, who helped me a lot during the whole master study, for their encouragement, insightful comments, and helpful suggestion.

I thank Dr. Shigeyuki Ishidoya and Dr. Shohei Murayama from AIST for providing the ground-based in situ CO_2 measurements data and Mr. Hidekazu Matsueda, Mr. Kazuhiro Tsuboi, and Mr. Yousuke Sawa from JMA for providing Meteorological tower CO_2 observing data.

I thank my fellow lab mates in room 310: Fuziwara san, Tiba san, Kino san and Iwakiri san, for the sleepless nights we were working together before deadlines, and for all the fun we have had in the last two years.

Last but not the least, I would like to thank my family: my parents Qiuping Lu and Zhongwei Cheng, for giving birth to me at the first place and supporting me spiritually throughout my life.